Thermal Microwave Foldover and Bistability in Ferromagnetic Resonance

Yuri K. Fetisov, *Senior Member, IEEE* and Carl E. Patton, *Fellow, IEEE*

***Abstract*—We investigated microwave foldover and bistability responses for a microwave resonator structure containing a 100-μm-thick yttrium iron garnet single-crystal film. We applied a static field of 3100 Oe perpendicular to the film plane, with continuous-wave and pulse microwave excitation at 4 to 5 GHz, and powers ranging from below 0 dBm up to 25 dBm. For input powers below 0 dBm, the main ferromagnetic resonance line was Lorentzian, centered at $f_0 = 4540$ MHz, and had a frequency width at half power of 17.6 MHz. Input powers above 0 dBm yielded nonlinear effects. For powers from 0 to 7 dBm, frequency sweeps gave distorted lines but no foldover. From 7 to 20 dBm, a hysteretic foldover response developed, with a gradual rise and a steep drop in absorbed power for up sweep and a cusp response on down sweep. We observed a corresponding nonlinear and bistability response when power sweep measurements were made at fixed frequency. The threshold frequency for bistability was about 15 MHz above f_0. The frequency shifts with power and the effect of changes in the sweep rate or pulse duty cycle indicate a thermal origin of these power-dependent nonlinear responses. All of the results could be accurately modeled though a resonance analysis in which the mode frequency f_r changed with the absorbed power P_a according to $f_r = f_0 + BP_a$, with $B = 1.83$ MHz/mW from the frequency shift data.**

***Index Terms*—Magnetic films, magnetic resonance, magnetostatic waves, nonlinear resonator.**

I. Introduction

FERRITE materials with microwave excitation at high power levels exhibit strong nonlinear effects that are important from a physical point of view and for microwave device applications. Two particular effects, "foldover" and "bistability," are often observed under conditions of ferromagnetic resonance (FMR) [1]–[10].

The foldover effect, initially observed by Weiss in 1958 [1] for a single crystal yttrium iron garnet (YIG) sphere, first appears as a reversible distortion in the FMR absorption profile at moderate powers, and then followed by a severe nonreversible distortion of the profile with a hysteretic character at high powers. These effects can be found for FMR loss profiles obtained as a function of magnetic field at fixed frequency or as a function of the frequency at fixed field. The control parameters here are the direction of the frequency or field sweep and the power. The effect can occur for spheres, in-plane magnetized films or slabs, and films of slabs magnetized perpendicular to the plane.

The related bistability effect [8]–[10] is realized when one selects an appropriate frequency and field combination, but then sweeps the microwave power up or down. In this case, one can have two different values of the output power for one and the same value of the input power and, hence, bistability. Here too, the control parameter is the direction of the sweep.

These foldover and bistability effects fall into two categories: 1) those which disappear if the measurements are made with pulses at low duty cycles and 2) those which remain. Category 1 processes are generally ascribed to heating and Category 2 to more intrinsic considerations. There have been numerous attempts to explain these effects. These attempts have met with limited success.

The most detailed work to date on the intrinsic response was done in [8]–[10]. These references also invoked a model based on a power-dependent mode frequency to calculate foldover and bistability responses for comparison with the data. The agreement, however, was qualitative at best. The overall conclusion was that the model, which follows the so-called dispersive nonlinearity approach in optics [11], cannot provide a quantitative account for the intrinsic foldover and bistability effects found in thin YIG films.

The work in [8]–[10] was for two film thicknesses, 4.9 and 25 μm. The objective in the present work was to extend the measurements to much thicker films where thermal effects are expected to dominate. Detailed data for foldover and bistability were obtained for a 100-μm-thick YIG film. The data were also examined in light of the dispersive nonlinearity model and a power-dependent mode frequency approach. Two new conclusions were obtained. First, measurements of the mode frequency shift as a function of power, sweep rate, and duty cycle indicated a thermal origin. Second, the model was found to give very good quantitative agreement with the data. This represents the first instance in the saga of FMR foldover and bistability investigations where any model has yielded quantitative agreement with experiment.

The measurements were performed on a YIG film magnetostatic wave (MSW) resonator, as in [8]–[10]. As the results show, the use of a 100-μm-thick film puts one well into the thermal regime of the microwave foldover and bistability responses. The measurements were carried out for both continuous-wave (CW) and pulse excitation in order to unambiguously confirm the thermal origin of the response. The thick-film

Manuscript received March 17, 2003; revised October 13, 2003. This work was performed at Colorado State University, and sponsored in part by the U.S. Army Research Office under Grants DAAG55-98-1-0430 and DAAD19-02-1-0197, the National Science Foundation under Grants DMR-9801649 and DMR-0108797, the Office of Naval Research under Grants N00014-94-1-0096 and N00014-03-1-0070, and the North Atlantic Treaty Organization (NATO) under Grant PST.CLG.978096.

Y. K. Fetisov is with the Moscow Institute of Radioengineering, Electronics and Automation (MIREA), 117454 Moscow, Russia (e-mail: fetisov@orc.ru).

C. E. Patton is with the Department of Physics, Colorado State University, Fort Collins, CO 80523 USA (e-mail: patton@lamar.colostate.edu).

Digital Object Identifier 10.1109/TMAG.2004.824132

0018-9464/04$20.00 © 2004 IEEE

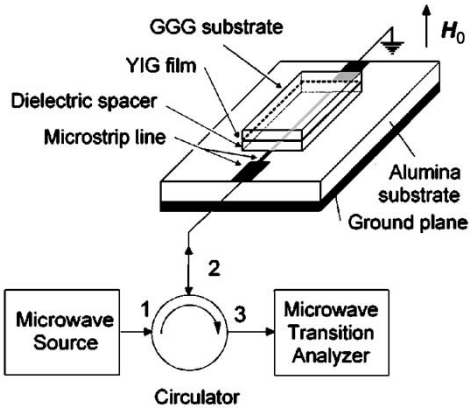

Fig. 1. Schematic of the YIG film resonator and the microwave measurement system. The film is upside down on a gadolinium gallium garnet (GGG) substrate and is separated from the microstrip line by a dielectric spacer. The static field $\boldsymbol{H}_0$ is applied perpendicular to the film plane.

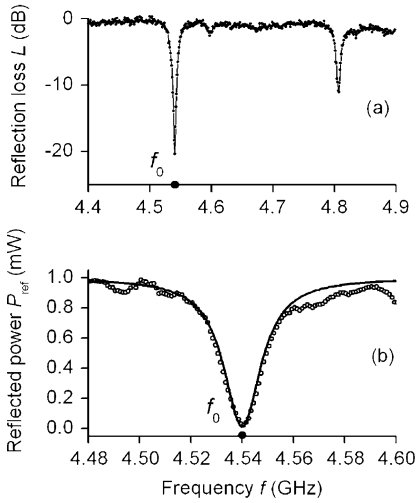

Fig. 2. Reflection loss L (a) and reflected power $P_{\rm ref}$ (b) as a function of the signal frequency for the YIG film resonator at a low input power level of 1 mW. The solid points in (a) show the complete wide-band frequency spectrum of the resonator. The solid line in (a) simply connects the points. The open circles in (b) show the main mode on an expanded frequency scale. The solid line in (b) shows a Lorentzian fit to the peak portion of the data. The main mode center frequency is indicated by the solid circle and the label f_0 in both panels.

effects occur for CW microwave excitation and *disappear* under low duty cycle pulse operation. This is *opposite* to the thin-film case in [8]–[10].

Computed responses were obtained from a specific model in which the resonance frequency f_r was taken to shift linearly with power according to $f_r = f_0 + BP_a$, where f_0 is the usual low-power FMR frequency, P_a is the absorbed power, and B is a scaling coefficient. (Note: all symbols and acronyms are listed and defined in the Appendix.) This is the same approach used in [8]–[10] and in work by Prabhakar and Stancil [12], except for the value and assumed origin of the coefficient B. This form gave empirical calibrations on the change in the saturation magnetization with P_a, which were consistent with a thermal origin of the foldover and bistable responses. In contrast with the poor correlation with theory for the intrinsic foldover effects in [8]–[10], the model yielded excellent quantitative agreement with the thick-film data.

The paper is organized as follows. Section II describes the YIG film resonator and the experimental setup. Section III presents the experimental results. Section IV describes the power-dependent frequency shift response model and gives a detailed comparison of the model predictions with the data.

II. YIG Film Resonator Setup

The measurements were made on a YIG film MSW resonator structure. Fig. 1 shows a schematic of the resonator and a block diagram of the instrumentation. The resonator consisted of a 100-μm-thick YIG film cut to make a 4 mm $\times$ 1 mm rectangular MSW resonator. The resonator was placed on top of the narrow section of a microstrip line with the long direction parallel to the line. The resonator was excited though a microwave source and a circulator. The reflected signals were analyzed with a microwave transition analyzer.

The YIG rectangle was cut from a single-crystal (111) film that was grown by standard liquid phase epitaxy methods on a 0.6-mm-thick gallium gadolinium garnet (GGG) substrate. The section of the microstrip line under the sample was 50 μm wide. This line made transitions to wider 50 Ω sections. One of these sections was shorted to ground. The other was used for input and output through the circulator. The YIG film was placed on the microstrip surface side down. A 100-μm-thick dielectric film was placed in between the film and the microstrip to decrease the coupling. The entire structure was placed in static magnetic field of 3100 Oe perpendicular to the film, as indicated by the arrow labeled H_0 in Fig. 1. This fixed field was used for all of the results given below.

The microwave source consisted of a Hewlett–Packard Model 83650A synthesized sweeper followed by a microwave amplifier. Microwave frequencies from 4 to 5 GHz were used. The circulator had a passband of 3–5 GHz, an insertion loss of about 2 dB, and an isolation of about 20 dB. The maximum input power at the resonator was +25 dBm, or 300 mW. The reflected signal was routed by the circulator to a Hewlett–Packard Model 70820A microwave transition analyzer. The data were collected and processed with a computer.

The setup was used in two measurement modes. In the first mode, the reflected power $P_{\rm ref}$ was recorded for sweeps of increasing and decreasing frequency for different levels for the input power $P_{\rm in}$. In the second mode, $P_{\rm ref}$ was measured for sweeps of increasing or decreasing $P_{\rm in}$ at fixed frequency. The rates for the frequency and power sweeps were varied from 2.6 to 42 MHz/s and from 0.16 to 2.6 dBm/s, respectively. Measurements were made with both CW and pulsed excitation. The pulsed measurements were made for pulse durations of 1–10 μs and a pulse repetition rate of 1 kHz.

III. Experimental Results

A. Low-Power Frequency Response

Fig. 2 shows a typical frequency response for the YIG film resonator with low-power excitation at $P_{\rm in}$ values below 1 mW (0 dBm). The data shown are for $P_{\rm in} = 1$ mW. Graph (a) shows the reflection loss L, expressed in decibel units as $L = 10\log(P_{\rm ref}/P_{\rm in})$, as a function of the signal frequency f. The

open circles in (b) show the main absorption peak on an expanded frequency scale. The solid line in (b) shows a Lorentzian fit to the main peak response region. The solid circle and label f_0 denote the main mode frequency in both graphs.

One can see from Fig. 2(a) that there are two absorption peaks. The main peak, which will be the focus of the measurements here, is centered at $f_0 = 4540$ MHz. The response was independent of the rate of the frequency sweep. This low-power response is purely linear. There are no nonlinear effects.

The low-power parameters that characterize the main peak will be important for the analysis in Section IV. The reflection loss at $f = f_0$ is -20 dB. This L value corresponds to a value of 0.99 for the ratio of the peak absorbed power $P_{\text{a-pk}}$ to P_{in}. This ratio will define an absorption parameter A. The full line width at half power for the main peak, taken as Δf, is 17.6 MHz. Note that [9] and [10] define Δf as *one half* of the full linewidth. The linewidth is about a factor of ten larger than the usual FMR linewidths for 5- to 10-μm-thick YIG films. The larger linewidth may be due to additional inclusions in the thick sample.

The Lorentzian fit to the expanded data for the main peak, as shown in Fig. 2(b), is based on

$$P_a = P_{\text{in}} \cdot \frac{A}{1 + \left(\frac{f - f_0}{\Delta f/2}\right)^2} \tag{1}$$

where P_a denotes the absorbed power. Note that (1) is valid under low power conditions with no nonlinear effects. The above form gives a good fit to the main peak response. In Section IV, the nonlinear response analysis will be based on the same form, but with f_0 replaced by a power-dependent resonance frequency.

The positions of the peaks in Fig. 2(a) are consistent with magnetostatic mode considerations, as in [8]–[10]. The appropriate modes for a perpendicular-to-plane magnetized ferrite film are standing magnetostatic forward volume wave (MSFVW) modes [13]. The lowest order MSFVW mode has a response that is essentially uniform over the film thickness and with an edge pinned standing mode pattern across the film rectangle. The main mode frequency may be written as

$$f_{\text{MSFVW}} \approx (|\gamma|/2\pi)(H_0 + H_A) - (|\gamma|/2\pi)\left[1 - \frac{1}{2}\left(\frac{d}{a} + \frac{d}{b}\right) + \frac{\pi d}{4}\sqrt{\frac{1}{a^2} + \frac{l}{b^2}}\right] 4\pi M_s \tag{2}$$

where γ is the electron gyromagnetic ratio for the ferrite, H_A is an effective anisotropy field for the [111] magnetized film, d is the film thickness, a and b are the lateral dimensions of the YIG rectangle, and $4\pi M_{\text{s}}$ is the saturation induction. For YIG, $|\gamma|/2\pi$ is approximately 2.8 GHz/Oe. The standard literature value of $4\pi M_{\text{s}}$ for yttrium iron garnet is 1750 G. These values will be used for the analysis below.

The main mode frequency scales with the applied field H_0 and the saturation induction. The $4\pi M_{\text{s}}$ factors in the square bracket term of (2), in order, are the thin-film demagnetizing factor of unity, a demagnetizing field correction for the finite size of the film [14], and a MSFVW mode correction term [13]. For the film dimensions given above, the square bracket factor is equal to 0.857 and the change in the mode frequency with $4\pi M_{\text{s}}$ is about -2.4 MHz/G. This is the response term that causes f_{MSFVW}, and the corresponding main resonance frequency f_0, to shift up with increasing power as the sample heats up and $4\pi M_s$ decreases.

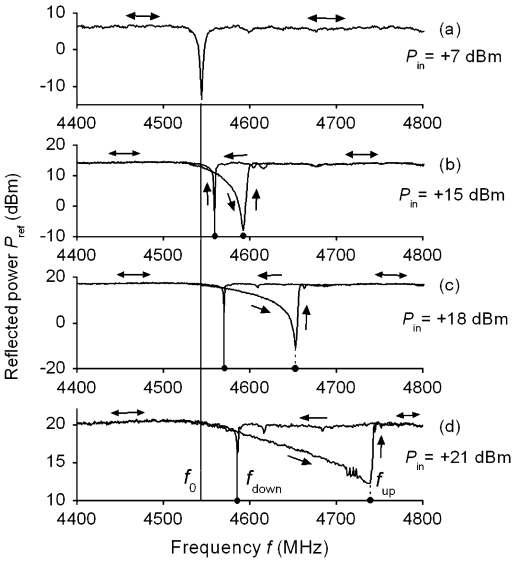

Fig. 3. Reflected power P_{ref} as a function of the frequency f for the YIG film resonator at various levels of input CW power P_{in}, as indicated. The arrows show the directions of the traces for the up-sweep and down-sweep profiles, as indicated. The vertical dotted line across all the panels shows the position of the main resonance at frequency for low power. The f_{up} and f_{down} frequency jump points for panels (b)–(d) are indicated by solid circles and dotted lines and labeled in panel (d) only.

Equation (2) accounts nicely for the measured main mode frequency at low power. If the main mode at $f_0 = 4540$ MHz is taken as equal to f_{MSFVW}, one obtains an empirical value of 20.4 Oe for the anisotropy field parameter H_A. This value is on the same order as the cubic magnetocrystalline anisotropy H_A value of about 36 Oe obtained from the standard FMR analysis for a perpendicular-to-plane magnetized (111) YIG film. The small difference is most likely due to additional stress related uniaxial anisotropy, inhomogeneous internal fields, a $4\pi M_s$ that is slightly different from the standard YIG value of 1750 G, or some combination of these effects.

B. Foldover Response

Fig. 3 shows typical measured reflected power versus frequency profiles for the YIG film resonator at four different P_{in} levels, as indicated. These particular data were obtained for a frequency sweep rate of 6.66 MHz/s. The up-sweep data for increasing frequency and the down-sweep data for decreasing frequency are indicated by the arrows adjacent to the curves. The vertical dotted line across all the graphs indicates the low-power main resonance peak position at $f = f_0$. Graphs (b), (c), and (d) also show solid circles on the frequency axis that indicate frequency jump points f_{up} and f_{down}, which are discussed and defined below. These f_{up} and f_{down} points are labeled in graph (d) only.

The data in Fig. 3 show the characteristic thermal foldover response. The trace for $P_{\text{in}} = +7$ dBm in (a) shows a small shift and an asymmetric distortion from the narrow and symmetric main peak profile in Fig. 2. These changes develop more or less

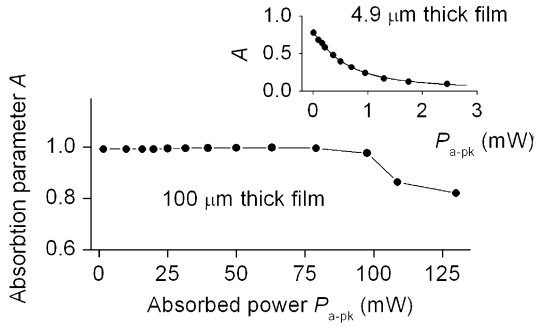

Fig. 4. Absorption ratio parameter A as a function of the maximum absorbed power $P_{\text{a-pk}}$ for the YIG film resonator. The insert in the upper right corner of the figure shows the corresponding result for a much thinner 4.9-μm-thick film from [9].

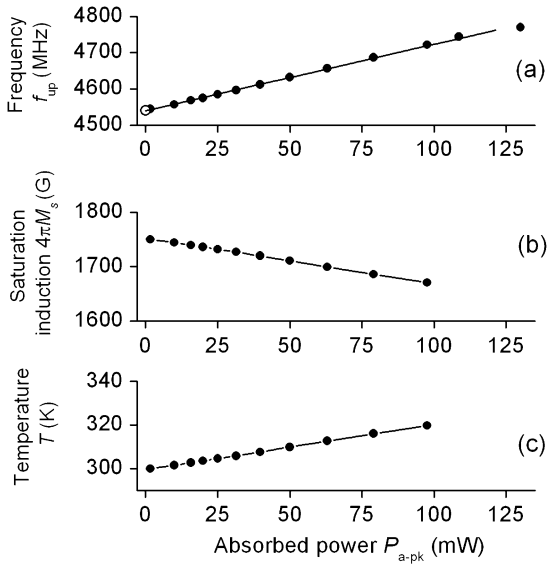

Fig. 5. (a) Measured jump frequency f_{up} versus peak absorbed power $P_{\text{a-pk}}$, shown by the solid circles, the main resonance frequency f_0 in the low power limit, shown by the open circle, and a linear fit to the f_{up} data with the two points at the highest powers excluded, shown by the solid line. (b) Saturation induction $4\pi M_s$ versus $P_{\text{a-pk}}$, based on the f_{up} shift with power in (a). (c) The temperature T versus $P_{\text{a-pk}}$, based on the $4\pi M_s$ response in (b) and the known $4\pi M_s(T)$ response. The lines in (b) and (c) simply connect the points. For (b) and (c), the two highest power points are excluded.

continuously as the power is increased from the low-power reference level of 1 mW (0 dBm). There is no hysteresis.

As soon as the power is increased above +7 dBm, one finds several abrupt and discontinuous changes from the trace shown in (a). There is a splitting in the up-sweep and down-sweep traces and the appearance of hysteresis. As the power is increased, the up-sweep trace also develops a very large asymmetry, continues to shift up in frequency, and the high-frequency edge of the profile becomes very sharp. At the same time, the down-sweep traces change to show only a sharp cusp response that shifts to higher frequency as P_{in} is increased. The down-sweep cusps always remain well below the steep high-frequency edge of the up-sweep traces.

The thermal foldover effects evident in Fig. 3 can be quantified through further measurements of the absorption ratio A and the two jump point frequencies f_{up} and f_{down} as a function of power. It will prove useful to show these dependences as a function of the peak absorbed power $P_{\text{a-pk}}$. This is because of the connection with heating and the frequency connection $f_r = f_0 + BP_a$ given in the introduction.

First, consider the change in the power ratio parameter $A = P_{\text{a-pk}}/P_{\text{in}}$ with $P_{\text{a-pk}}$. In Section III-A, the $P_{\text{a-pk}}$ parameter corresponded to the maximum in absorbed power at $f = f_0$ for low power measurements. This definition must now be modified. It is clear from Fig. 3 that for increasing power, the maximum absorbed power $P_{\text{a-pk}}$ will correspond to the P_a value *just before* the abrupt drop at $f = f_{\text{up}}$. The data show that the corresponding $P_{\text{a-pk}}/P_{\text{in}}$ ratio stays very close to the low-power limit value of 0.99 until the input power level exceeds about +20 dBm, or 100 mW. There is a drop in $P_{\text{a-pk}}/P_{\text{in}}$ only for P_{in} or $P_{\text{a-pk}}$ levels above 100 mW or so.

Fig. 4 shows the measured A versus $P_{\text{a-pk}}$ response. The main graph shows the variation in A with $P_{\text{a-pk}}$ over a range of values from 1.6 to 130 mW. The A ratios were obtained from up-sweep data similar to those in Fig. 3. Keep in mind that for $A \sim 1, P_{\text{a-pk}}$, and P_{in} are essentially equivalent. The upper right inset shows the corresponding A versus $P_{\text{a-pk}}$ response for a resonator with a much thinner 4.9-μm-thick film. The inset data are from Fig. 2 in [9].

The data in the main graph verify the basic result noted above. These results show that for the *thick-film resonator case*, there is no appreciable change in the $P_{\text{a-pk}}/P_{\text{in}}$ ratio over a wide range of $P_{\text{a-pk}}$ values from 1 mW up to almost 100 mW, a span of 20 dB. Over this full range, the A ratio remains constant at about 0.99. Only for $P_{\text{a-pk}}$ values above 100 mW or so does one find a drop in the $P_{\text{a-pk}}/P_{\text{in}}$ power ratio. From the data, one can see that A drops to about 0.8 at $P_{\text{a-pk}} \sim 130$ mW, or for $P_{\text{in}} \sim 130\ \text{mW}/0.8 \sim 160$ mW. This drop may be attributed to the onset of intrinsic nonlinear effects, as in [9]. Further comments on intrinsic high power effects for thick films are given below.

In addition to the drop in the A-ratio with power for the thick films for $P_{\text{in}} > 100$ mW, there are additional intrinsic nonlinear effects. These are evident from Fig. 3(d) for $P_{\text{in}} = +21$ dBm $\sim$ 126 mW. Just before the jump at $f = f_{\text{up}} \sim 4750$ MHz, one sees some additional structure in the form of a small region of oscillation. This oscillation region expands if the power is increased further. This effect is reminiscent of the well-known relaxation oscillations or modulational instability effects that often accompany intrinsic nonlinear effects.

The inset data in Fig. 4 show the contrast in the A versus $P_{\text{a-pk}}$ response for *the case of a thin film*. Here, there is a rapid drop in A with increasing $P_{\text{a-pk}}$. A plot of A versus P_{in} instead of $P_{\text{a-pk}}$ would drop even faster. This drop also occurs for much smaller values of $P_{\text{a-pk}}$ than for the thick-film case. As discussed in [9], this response is related to intrinsic foldover effects.

The constant A values for $P_{\text{a-pk}} < 100$ mW provides one indication of a thermal effect. The frequency jump data provide additional support for a thermal process. Fig. 5 shows the change in the up-sweep jump frequency f_{up} with the absorbed power $P_{\text{a-pk}}$, along with calculated variations in the saturation induction $4\pi M_s$ and the thin-film temperature T with $P_{\text{a-pk}}$ based on these data. The calculations were based on the assumption that the frequency shifts derive from a decrease in $4\pi M_s$ due to heating.

Graph (a) in Fig. 5 shows the f_{up} data as solid circles. The single open circle point indicates the low-power main resonance

frequency value at f_0. The straight line in the graph corresponds to a best fit to the $f_{\rm up}$ data with the two highest power data points excluded. These last two points were excluded from the fit because of the onset of nonlinear effects noted above. The $4\pi M_s$ versus $P_{\text{a-pk}}$ points in (b) were obtained from the data in (a) and the $f_{\rm MSFVW}$ versus $4\pi M_s$ response from (2) with $f_{\rm MSFVW}$ replaced with $f_{\rm up}$ or f_0, as appropriate. The T versus $P_{\text{a-pk}}$ results in (c) were obtained from the points in (b) and a room temperature $d(4\pi M_s)/dT$ slope of 3.8 G/K as estimated from [15]. The lines in (b) and (c) connect the points. As with (a), the two highest power points are excluded.

The $f_{\rm up}$ versus $P_{\text{a-pk}}$ data in Fig. 5(a) provide the empirical basis for power-frequency connection noted in the introduction. The data indicate a linear response of the form

$$f_{\rm up} = f_0 + BP_{\text{a-pk}}. \tag{3}$$

The fit in (a) has a slope of 1.83 MHz/mW. The analysis in Section IV will take this empirical response to apply to the more general shift in the frequency f_r with the absorbed power P_a even when one is not at the FMR peak.

A power frequency response of the form in (3) does not, in itself, prove that the foldover has a thermal origin. The main evidence for thermal foldover will come from the duty cycle and pulse results in Section III-D. The responses in graphs (b) and (c) of Fig. 5 do show, however, that the assumption of a thermal response gives reasonable values for the changes in both $4\pi M_s$ and temperature T with absorbed power. The slope of the line in Fig. 5(b) is essentially the slope of the (a) fit divided by the 2.4 MHz/G $f_{\rm MSFVW}$ versus $4\pi M_s$ response from (2). This gives 0.8 G/mW. This implies a change in $4\pi M_s$ of about 80 G over the range of $P_{\text{a-pk}}$ values in the graph. The corresponding slope in graph (c) is about 0.2 K/mW. Both of these responses are reasonable for a thermal effect.

The thermal response times are also reasonable. The sweep rate of 6.66 MHz/s for the data in Fig. 3 and the 2–5 MHz width of the frequency jumps and cusps suggest a response time somewhat less than 1 s. This is consistent with a thermal process. As noted in [10], intrinsic foldover and bistability responses have time constants that are in the range of a few microseconds, the same as the intrinsic relaxation rate. Further data on sweep rate and duty cycle effects are given in Section III-D.

The data show that the shift in $f_{\rm up}$ with $P_{\text{a-pk}}$ deviates somewhat from the linear response shown in Fig. 5(a) for $P_{\text{a-pk}}$ and $P_{\rm in}$ values above 100 mW. Although not shown in Fig. 5, additional data up to $P_{\rm in}$ levels of 300 mW show very large deviations in the $f_{\rm up}$ response from the linear fit. These deviations are accompanied by the strong decrease in the A parameter already noted. In addition to these changes, the actual shapes of the up-sweep absorption profiles become much more complicated than shown in Fig. 3. Among other things, the profiles develop a large expansion in the oscillatory feature shown in Fig. 3(d). These very high power effects are clearly beyond the realm of thermal considerations.

C. Bistability

As discussed in the introduction, one may also make measurements for up sweeps or down sweeps in the input power at fixed frequency. As with the frequency sweeps at fixed power, the reflected power versus input power profiles also give a hysteretic response with jumps and cusps at particular power points on the up-sweep and down-sweep curves. In this mode, however, one has a *bistable* power response. One can have *two different values* of the reflected power for a given value of the input power, depending on whether one is on the up-sweep or the down-sweep part of the response.

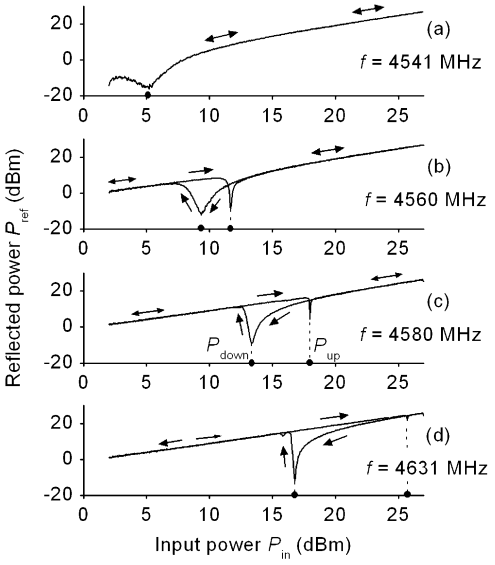

Fig. 6. Reflected power $P_{\rm ref}$ as a function of input power $P_{\rm in}$ at different operating frequency f points, as indicated. The arrows show the direction of the sweeps. The $P_{\rm up}$ and $P_{\rm down}$ jump points for (b)–(d) are indicated by solid circles, but are labeled in (c) only.

Fig. 6 shows typical thick-film bistability results. The graphs show up-sweep and down-sweep profiles for the reflected power $P_{\rm ref}$ as a function of the incident power $P_{\rm in}$ for a series of f values, as indicated. In (a), f is only 1 MHz above the f_0 main resonance point at low power. For (d), f is more than 90 MHz above f_0. The range of the $P_{\rm in}$ values on the horizontal axes range from 2 dBm to about +27 dBm, somewhat greater than the $P_{\rm in} = +21$ dBm level for graph (d) of Fig. 3. As in Fig. 3, arrows indicate the directions of the sweeps and solid circles indicate jump points. The jump point labels for the up-sweep cusps and down-sweep shoulders are indicated by the $P_{\rm up}$ and $P_{\rm down}$ parameters in (c) only. All profiles in Fig. 6 were obtained for a $P_{\rm in}$ sweep rate of 0.33 dBm/s.

The features of the bistable response are similar to those found in foldover. If the signal frequency f is only slightly above f_0, one obtains a distorted $P_{\rm ref}$ versus $P_{\rm in}$ response but no hysteresis. For larger and larger frequency shifts, as in (b)–(d), one obtains hysteretic behavior, cusps, and jumps. The main difference here is that the up-sweep and down-sweep effects are reversed and the hysteretic responses constitute bistability in power. A $P_{\rm in}$ up sweep gives a sharp cusp at some frequency-dependent $P_{\rm up}$ point. Down-sweep data give a gradual rise and then a jump at some $P_{\rm down}$. The larger the frequency shift above f_0, the higher the power points for the cusps and jumps. No curves are shown for $f < f_0$. In this case, the $P_{\rm ref}$ versus $P_{\rm in}$ response is simply linear.

Recall from the discussion of Fig. 3 that one needs some critical power level above about +7 dBm to obtain a hysteretic response. In the power sweep experiments, there is a corresponding frequency threshold. A reversible response as in (a) is obtained only if $f - f_0$ is less than about 16 MHz. The data in (b) for $f - f_0 = 20$ MHz, in contrast, show that the hysteresis is already substantial.

As one proceeds from (b) to (d) in Fig. 6, the bistable region in power shifts to a higher and higher $P_{\rm in}$ range and widens. This widening is evident from the roughly constant width of 3–5 dB for the hysteretic interval as one moves from (b) to (d). At higher powers, a given decibel range corresponds to a wider range in actual powers. Note also the apparent narrowing of the down-sweep dip and jump region as the frequency is increased. This is also a decibel effect. On a linear scale of power, the widths of these regions would be about the same.

The data also show that the up-sweep cusp jump point $P_{\rm up}$ shifts up in power rather rapidly as the frequency is increased, in contrast with the much smaller increases in the bistable power interval and the down-sweep $P_{\rm down}$ jump point. In (d), for example, the cusp has shifted almost to the end of the scale and is extremely small. Quantitative data on $P_{\rm up}$ and $P_{\rm down}$ as a function of the input power will be presented in Section V as part of the thermal foldover and bistability analysis.

As noted above, responses such as those in Fig. 6 require an operating point frequency that is *above* the f_0 main resonance point at low power. This is related to the fact that the shift in the resonance frequency of the main mode as the power is increased is always toward higher values for the perpendicular field configuration. Operating point frequencies below f_0 cannot give a nonlinear or bistable response. This is because any shift in the mode position due to heating will simply move the resonance up in frequency and farther away from the operating point. Experimentally, one finds only a linear change in $P_{\rm ref}$ with $P_{\rm in}$ for operating point frequencies below $f = f_0$. There is no distortion of the sort shown in Fig. 6(a) and no bistability effect of the sort shown in (b)–(d). This is related to the upshift in f_r relative to f_0 with power. There is no effect for f values *below* f_0.

In closing this section, it is important to comment on the differences between the "bistability" response for thick films and the corresponding response for thin films. As with foldover, the thick-film bistable effects are much larger than for thin films. The data in Fig. 6 show that the overall size of the changes in $P_{\rm ref}$ is in the 10–20 dB range and the width of the bistable region on the $P_{\rm in}$ axis is on the order of 5–10 dB. In the thin-film experiments, as in [8], the maximum change in $P_{\rm ref}$ was only a few decibels at most and the width of the bistable region in $P_{\rm in}$ was never more than 5 dB. The much larger thick-film bistable response lies in the thermal origin of the effect.

D. Sweep Rate and Pulsewidth/Duty Cycle Effects

This section discusses (1) the changes in the above responses as a function of the sweep rate and (2) the absence of any nonlinear effects for pulse measurements at a low duty cycle. Both sets of results provide further support for a thermal origin of the foldover and bistable effects presented above. First, consider the effect of a change in the frequency sweep rate on the foldover response. Thermal processes will give profiles and values of $f_{\rm up}$ and $f_{\rm down}$ that are independent of the sweep rate only if the rate of change is slow enough for the system to achieve thermal equilibrium at each frequency point.

The data in Fig. 3 were obtained for a frequency sweep rate of 6.6 MHz/s. Further data in the same format were obtained for a wide range of sweep rates from 2.6 to 42 MHz/s. For rates from 2.6 to 10 MHz/s, the data were essentially unchanged from those in Fig. 3. However, as the sweep rate was increased from 10 to 42 MHz/s, two changes were observed. First, it was found that the increasing sweep rate caused the up-sweep frequency jump point $f_{\rm up}$ to gradually fall back to lower f values. The actual "jump" also became more gradual. Second, it was found that the down-sweep cusp at $f = f_{\rm down}$ became smaller. The higher sweep rates caused no change in either the up-sweep shoulder response that precedes the $f_{\rm up}$ jump or the position of the down-sweep cusp.

Changes in the power sweep rate produced analogous changes in the bistable response. For rates from 0.16 to 0.5 dBm/s, the data were the same as in Fig. 6. As the power sweep rate was increased from 0.5 to 2.6 dBm/s, however, there was a gradual up-shift in the down-sweep jump point $P_{\rm down}$, a narrowing of the bistability region width in $P_{\rm in}$, and a decrease in size of the jumps and cusps.

The above results show that frequency sweep rates below 10 MHz/s and power sweep rates below 0.5 dBm/s are sufficiently slow to maintain thermal equilibrium during the up-sweep and down-sweep measurements. Recall that the low power linewidth for the main resonance is 17.6 MHz. This linewidth, divided by the 10 MHz/s frequency sweep limit for a thermal lag, gives a characteristic time of about 2 s. The widths of the jumps and cusps in Fig. 3 also give thermal response times on the order of 1 s.

These thermal responses are consistent with recent data on the transient microwave response of ferrite films subjected to pulsed laser heating [16]. Those data give characteristic cooling times that are on the order of several seconds. The data also show that the characteristic times for heating are very short, on the order of nanoseconds or less. This is consistent with the thermal effects seen here. The cooling times match the time estimates above. The lack of any observed changes in the gradual upsweep profiles *before* the $f_{\rm up}$ jump points or in the positions of the down-sweep cusps as the sweep rate is increased suggests that heating times in the present experiments were essentially instantaneous, as found in [16].

Finally, consider the pulse measurements at low duty cycle. Pulse data were obtained for pulsewidths in the 1–10 μs range and a repetition rate of 1 kHz. From the low power linewidth of 17.6 MHz, the intrinsic FMR response time is well below 1 μs, and the 1–10 μs pulsewidths are sufficient to achieve a steady-state precession response. These pulsewidths, in combination with the relatively low 1-kHz repetition rate, give duty cycles in the 0.1%–1% range, low enough to avoid measurable heating effects.

Under these low duty cycle conditions, one would expect to see *no foldover* and *no bistability* effects. This expectation was confirmed by the data. Up and down frequency sweep data at pulse power levels *up to* +20 dBm gave FMR profiles *which*

matched precisely to the low power curves in Fig. 2. These high power pulse data showed no nonlinear response, no foldover, and no cusp effects. Corresponding power sweep data at fixed frequency also gave a linear response, with no regions of bistability or cusps.

IV. Response Analysis

A. Nonlinear Response Model

As noted above, the foldover and bistability response model used here is based on the dispersive nonlinearity model, which is well known in optics [11]. Use of the model for YIG film resonators structure was discussed in [8]–[10] and in [12]. The procedure is straightforward. One needs only to take the power versus frequency resonance response of (1), replace the fixed mode frequency f_0 in this response equation with the power-dependent mode frequency f_r, and solve for the absorbed power P_a versus frequency f or input power $P_{\rm in}$.

Reference [8] gives a full discussion of the analysis procedure. Only the basic working equations will be given below. In the thin-film case considered in [8], however, there were wide differences between the computed response and the thin-film data. For this intrinsic foldover situation with no duty cycle or heating effects, it was not possible to obtain even a qualitative match with the measured foldover response profiles or jump points as a function of frequency. In the thick-film case considered here, in contrast, one obtains a near perfect match for both the foldover and the bistability response profiles, and for the jump and cusp point values. These detailed comparisons are given in Section IV-B.

The working equation for the absorbed power P_a versus frequency f follows the form of (1) and is written as

$$P_a = P_{\rm in} \cdot \frac{A}{1 + \left(\frac{f - f_r}{\Delta f/2}\right)^2}. \tag{4}$$

Recall that P_a denotes the absorbed power, A is the ratio of the peak in the absorbed power $P_{\rm a\text{-}pk}$ to the input power $P_{\rm in}$, and Δf is the half power frequency linewidth at low power. Equation (4) is of the same form as the low-power FMR response of (1) in Section III, except for the replacement of f_0 with the power-dependent frequency f_r. This replacement is all that is needed to accurately model *all* of the thermal foldover data in the current experiments.

Based on the frequency shift data in Fig. 5, the power-dependent main resonance frequency f_r is taken to have the form

$$f_r = f_0 + BP_a. \tag{5}$$

This form is taken from (3), $f_{\rm up} = f_0 + BP_{\rm a\text{-}pk}$, with $f_{\rm up}$ replaced by f_r and $P_{\rm a\text{-}pk}$ replaced by P_a. This changeover forms the basis of the model. It is based on two significant assumptions. First, and as discussed in Section III, one takes the jump at the $f = f_{\rm up}$ as the actual main mode peak frequency at that power point, namely, $P_{\rm a\text{-}pk}$. Second, and most significant, one takes the $f_{\rm up}$ versus $P_{\rm a\text{-}pk}$ response as a *general measure* of the change in f_r with the absorbed power P_a *even when one is off the resonance peak*.

The fixed parameters in (4) and (5) derive from the data, as already noted. The low-power FMR fits in Section III-A gave an f_0 value of 4540 MHz and a Δf value of 17.6 MHz. The high power swept frequency data in Section III-B gave A and B values of 0.99 and 1.83 MHz/mW, respectively. These A and B parameters apply only for absorbed power levels below about 100 mW or so. Intrinsic nonlinear effects become important for higher powers.

If one replaces the f_r in (4) with the $f_0 + BP_a$ expression from (5), one obtains a cubic equation in P_a

$$B^2P_a^3 - 2(f - f_0)BP_a^2 + \left[(f - f_0)^2 + \left(\frac{\Delta f}{2}\right)^2\right] P_{\rm a} - AP_{\rm in} = 0. \tag{6}$$

For a given value of the frequency f and the input power $P_{\rm in}$, one may have either one or three real root values for the absorbed power.

The behavior of the P_a root solutions to (6) establish the theoretical conditions for foldover and bistability. It turns out, for example, that there is a threshold input power $P_{\rm th}$ below which there is only one real P_a root for *any frequency*. For $P_{\rm in} > P_{\rm th}$, there are three real roots for frequencies between limits that correspond to $f_{\rm down}$ and $f_{\rm up}$. Outside of these limits, there is also only one real P_a root. One obtains a foldover response for $f_{\rm down} < f < f_{\rm up}$. The $P_{\rm th}$ threshold power is given by

$$P_{\rm th} = \frac{8\sqrt{3}}{9}\frac{\Delta f/2}{AB}. \tag{7}$$

For the parameter values cited above, one obtains $P_{\rm th} = 7.48$ mW.

Similarly, there is a limit frequency $f_{\rm min}$ below which there is only one real P_a root for any power. For $f > f_{\rm min}$, there is an interval of input powers defined by $P_{\rm down} < P_{\rm in} < P_{\rm up}$ for which there are three real P_a roots. Outside of this interval, there is only one real root. This $P_{\rm in}$ interval corresponds to a bistable response. The $f_{\rm min}$ limit frequency is given by

$$f_{\rm min} = f_0 + \frac{\sqrt{3}}{2}\Delta f. \tag{8}$$

For $f_0 = 4540$ MHz and $\Delta f = 17.6$ MHz, one obtains $f_{\rm min} = 4555.5$ MHz.

The above responses are best illustrated by way of example. Fig. 7 gives representative results for the real P_a roots as a function of the operating point frequency f and input power $P_{\rm in}$. Except for curve 1 in (b), all of the computations were done for the $f_0, \Delta f, A$, and B values given above. For curve 1 in (b), B was set to zero. The curves in (a) show the real P_a root solutions versus f at different values of $P_{\rm in}$, as indicated. Curve 1 is for a $P_{\rm in}$ value below the $P_{\rm th}$ threshold for foldover. Curve 2 is for $P_{\rm in} \approx P_{\rm th}$. Curve 3 is for a $P_{\rm in}$ value well above the foldover threshold. Curve 1 in graph (b) is for $f = f_0 = 4540$ MHz and, as noted above, $B = 0$. Curve 2 is for $f = f_{\rm min} = 4555.5$ MHz, just at the bistability limit. Curve 3 is for $f = 4570$ MHz. The up and down jump points in frequency and power that correspond to the parameters introduced in Section III are also shown.

The curves in Fig. 7 demonstrate how the foldover and bistability responses come about. Curve 1 in (a) shows a typical loss

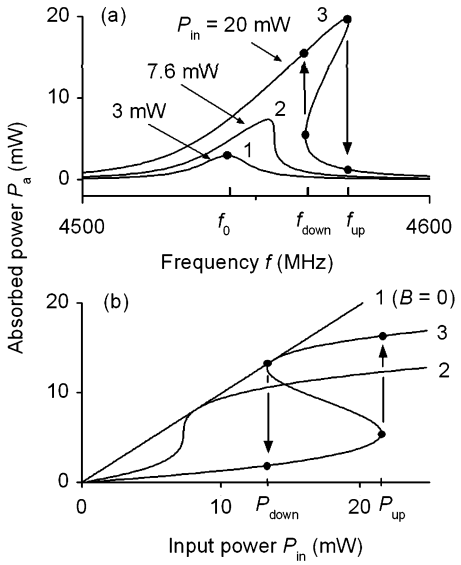

Fig. 7. Graphs (a) and (b) show calculated foldover and bistability profiles of the absorbed power P_a versus frequency f and the input power $P_{\rm in}$, respectively. All curves were obtained for a peak power absorption ratio $A = 0.99$, a low-power main mode frequency $f_0 = 4540$ MHz, and a low-power linewidth $\Delta f = 17.6$ MHz. Curves 1, 2, and 3 in (a) and curves 2 and 3 in (b) are for a power frequency response parameter $B = 1.83$ MHz/mW. Curve 1 in (b) is for $B = 0$. The $P_{\rm in}$ values for the curves in (a) are as indicated. For curve 3, the frequency limits $f_{\rm up}$ and $f_{\rm down}$ for the foldover region are indicated. Curves 1, 2, and 3 in (b) are for values of 4540, 4555.2, and 4570 MHz, respectively. For curve 3, the $P_{\rm in}$ limits $P_{\rm up}$ and $P_{\rm down}$ for the bistability region are indicated.

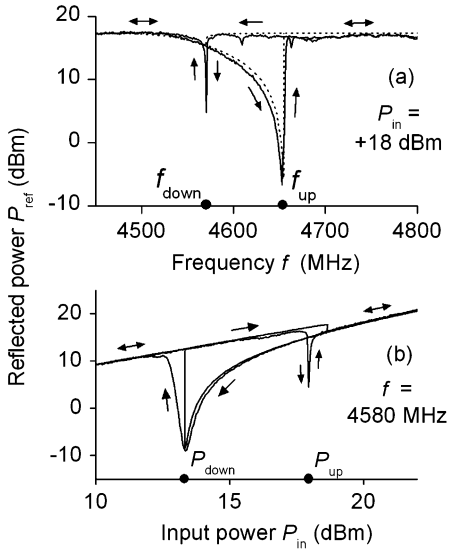

Fig. 8. Graphs (a) and (b) show foldover and bistability response profiles of reflected power $P_{\rm ref}$ versus frequency f and input power $P_{\rm in}$, respectively. The noisy traces show data and the smooth traces show the calculations. Up-sweep and down-sweep profiles are indicated by the arrows. The profiles are for fixed power or fixed frequency, as indicated. The up and down frequency and power jump points are indicated on the horizontal axes.

versus frequency response for $P_{\rm in} < P_{\rm th}$. In this range, one finds an upward shift in frequency and a growing distortion in the response profile but only one real P_a root at any given f. Curve 2 shows the limit of this response at $P_{\rm in} = 7.6$ mW $\approx P_{\rm th}$. Here, the profile is distorted to the point of showing a vertical slope on the high-frequency side of the response.

Curve 3 shows the foldover response that is obtained for $P_{\rm in} > P_{\rm th}$. One now has an interval in frequency for which there are three real P_a root solutions. Within this interval, one obtains a characteristic "folded over" response. For an up sweep in frequency, one obtains an abrupt drop in P_a at points corresponding to $f = f_{\rm up}$. For a down sweep, one obtains a cusp effect at points corresponding to $f = f_{\rm down}$. One gets a cusp because the frequency f is moving down while the mode frequency f_r is moving up. The FMR line is, in effect, moving through the operating point frequency and this gives a cusp response.

There is a similar scenario for bistability. Curve 1 in Fig. 7(b), for $f = f_0 = 4540$ MHz and $B = 0$, demonstrates the purely linear response that is obtained when there is no nonlinear shift in the main mode frequency with power. Curves 2 and 3 show the effect of a nonzero B on the P_a versus $P_{\rm in}$ response. The $f = f_{\rm min} = 4555.2$ MHz condition for curve 2 demonstrates the transition from a reversible nonlinear response to bistability. For f values between f_0 and $f_{\rm min}$, one has only one real root solution for P_a. A nonzero B will produce a distorted response but there will be no bistability. At the curve 2 limit, the vertical slope on the high power side of the response marks the transition to a bistable response.

If f is above $f_{\rm min}$, as for curve 3 in (b), one obtains a characteristic "S" shaped P_a versus $P_{\rm in}$ response. There is a region in power, $P_{\rm down} < P_{\rm in} < P_{\rm up}$, for which there are three real P_a roots. For an increase in $P_{\rm in}$ from low values, one follows the lower part of the S response up to $P_{\rm in} = P_{\rm up}$. As $P_{\rm in}$ moves above $P_{\rm up}$, the response then jumps to the upper part of the S, as indicated. Similarly, for a decreasing power from some high value, one follows the upper part of the S response, and then jumps back to the lower part at $P_{\rm in} = P_{\rm down}$. The overall effect is a P_a versus $P_{\rm in}$ response with a bistable character. The bistable cusp response is now found at the power up-sweep jump.

B. Comparisons With Experiment

The model gives threshold power and frequency values, response profiles, and jump and cusp points that closely match the data. The first point of comparison is for the $P_{\rm th}$ and $f_{\rm min}$ parameters from (7) and (8). The numerical values of A, B, and Δf from the fits in Section III give $P_{\rm th}$ and $f_{\rm min}$ values of 7.48 mW and 4555.2 MHz, respectively. Also from Section III, the experimental input power needed to achieve foldover was a little higher than +7 dBm, or about 5 mW. Fig. 6 shows, moreover, that at $f = 4560$ MHz, the bistable response is already well developed. These observations are consistent with the theoretical limits from the model.

The second point of comparison is for the P_a versus f and P_a versus $P_{\rm in}$ profiles. Fig. 8 shows representative results. Graphs (a) and (b) follow the formats of Figs. 3 and 6, respectively. Arrows indicate the directions of the sweeps. The curves in (a) and (b) were obtained for $P_{\rm in} = 18$ dBm and $f = 4580$ MHz, respectively. The noisy traces show the measurements and the smooth traces show the calculations. The frequency and power jump and cusp points from the data are indicated. There is an extremely good match between theory and experiment. The jump

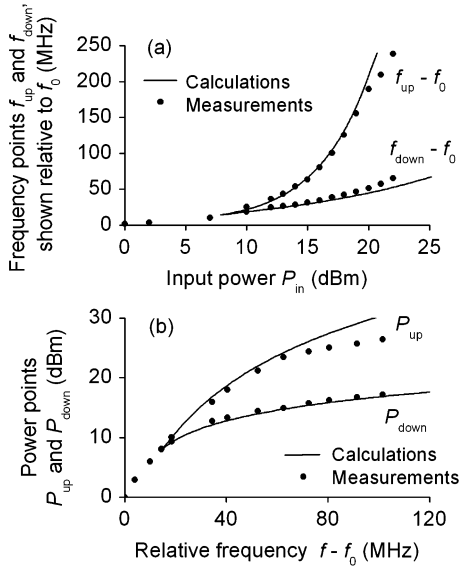

Fig. 9. Graph (a) shows measured and calculated frequency jump and cusp points $f_{\rm up}$ and $f_{\rm down}$ as a function of the input power $P_{\rm in}$. Graph (b) shows measured and calculated power jump and cusp points $P_{\rm up}$ and $P_{\rm down}$ as a function of the frequency f. All frequencies are shown relative to the low-power main mode frequency $f_0 = 4540$ MHz.

and cusp points match closely, as do essentially the entire profiles for both up sweep and down sweep.

The third point of comparison is for the jump and cusp points. Fig. 9 shows these results. Graph (a) shows the up-sweep and down-sweep frequency jump and cusp points $f_{\rm up}$ and $f_{\rm down}$ from the foldover profiles as a function of the input power $P_{\rm in}$. Graph (b) shows the corresponding bistability jump and cusp points in power, $P_{\rm up}$ and $P_{\rm down}$, as a function of frequency. The vertical and horizontal frequency scales in (a) and (b), respectively, show frequencies relative to the main mode frequency at low-power f_0, as indicated. The solid circles show the data and the solid lines show the calculations.

As with Fig. 8, the matchup between the calculated and measured frequency and power jump points is extremely good. The results in (a) show extremely good agreement out to an input power limit of 20 dBm, or 100 mW, where intrinsic effects come into play. The results in (b) show that both of the calculated power jump points match the data out to $f - f_0$ values of about 60 MHz, and the $P_{\rm down}$ results match out to the limit of the measurements at $f - f_0 \approx 100$ MHz.

The results in Fig. 9 provide a further demonstration of the $P_{\rm th}$ and $f_{\rm min}$ threshold conditions discussed above. In (a), both the calculated and measured frequency jump points come together for input power levels below about 7–8 dBm, and this convergence corresponds to the $P_{\rm th}$ from (7). In (b), the power jump points come together when $f - f_0$ is less that about 15 MHz. This convergence corresponds to the $f_{\rm min}$ from (8).

V. Summary and Conclusion

The foldover and bistability response profiles for a thick YIG film ferromagnetic resonance resonator have been measured as a function of frequency and power, respectively, for both CW and pulse excitation. The frequency changes with power, as well as the widths of the foldover frequency jumps and cusps, were found to be consistent with thermal effects. The disappearance of all of these effects under low duty cycle pulse measurements confirm the thermal origin of the responses.

Fits to the low-power FMR response and the peak frequency shift with power were used as the basis for mode profile and jump point calculations. The model gave threshold powers and frequencies, foldover and bistability profiles, and jump and cusp points that were in excellent quantitative agreement with the measurements.

These thick-film results represent the first comprehensive data for thermal foldover and bistability in a ferrite system. They also constitute the first successful theoretical analysis of such effects based on the dispersive nonlinearity power frequency shift model.

Appendix
Definitions of Symbols and Acronyms (in Order of Appearance)

FMR	Ferromagnetic resonance.
YIG	Yttrium iron garnet.
f_r	Power-dependent main resonance peak frequency.
f_0	Main resonance peak frequency at low power.
$P_{\rm a\text{-}pk}$	Absorbed power at peak of the main resonance.
B	Main resonance peak frequency power response coefficient, in $f_r = f_0 + BP_{\rm a\text{-}pk}$.
MSW	Magnetostatic wave.
GGG	Gadolinium gallium garnet.
H_0	Static external magnetic field applied perpendicular to the YIG film plane.
$P_{\rm ref}$	Power reflected from YIG film stripline excitation structure connection port.
$P_{\rm in}$	Input power to the YIG film stripline excitation structure at the connection port.
L	Reflection loss defined by $L = 10\log(P_{\rm ref}/P_{\rm in})$.
f	Signal frequency.
A	Absorption coefficient defined by $A = P_{\rm a\text{-}pk}/P_{\rm in}$.
Δf	Full linewidth at half power for the main FMR peak as measured at low power.
MSFVW	Magnetostatic forward volume wave.
$f_{\rm MSFVW}$	Lowest order MSFVW mode frequency.
γ	Electron gyromagnetic ratio for the YIG material ($\lvert\gamma\rvert/2\pi = 2.8$ GHz/kOe).
H_A	Effective anisotropy field for the YIG film ($H_A \sim 20.4$).
d	YIG film thickness ($d = 100$ μm).
a	Length of long side of YIG film rectangular sample.
b	Length of short side of YIG film rectangular sample.
$4\pi M_{\rm s}$	Saturation induction (in G) for the YIG material ($4\pi M_{\rm s}$ taken as 1750 G).
P_a	Absorbed power (at any power).
$f_{\rm up}$	Point in frequency on an up-sweep reflected power versus frequency profile at which there is an abrupt increase in the reflected power.
$f_{\rm down}$	Point in frequency on a down-sweep reflected power versus frequency profile at which there is an abrupt cusp (decreasing $P_{\rm ref}$) in the reflected power.

T Temperature.
$P_{\rm up}$ Point in input power on an up-sweep reflected power versus input power profile at which there is an abrupt cusp (decreasing $P_{\rm ref}$) in the reflected power.
$P_{\rm down}$ Point in input power on a down up-sweep reflected power versus input power profile at which there is an abrupt increase in the reflected power.
$P_{\rm th}$ Input power threshold for the realization of foldover in a swept frequency experiment.
$f_{\rm min}$ Minimum frequency for the realization of bistability in a swept power experiment.

ACKNOWLEDGMENT

The authors acknowledge Prof. J. Pelzl, Dr. V. T. Synogatch, and Dr. M. M. Scott for useful discussions.

REFERENCES

[1] M. T. Weiss, "Microwave and low-frequency oscillations due to resonance instabilities in ferrites," *Phys. Rev. Lett.*, vol. 1, pp. 239–241, Oct. 1958.
[2] J. I. Masters, "Instability of magnetic resonance in single crystal spheres of yttrium iron garnet," *J. Appl. Phys.*, vol. 31, pp. 41S–42S, 1960.
[3] K. D. McKinstry, C. E. Patton, and M. V. Kogekar, "Low power nonlinear effects in the ferromagnetic resonance of yttrium iron garnet," *J. Appl. Phys.*, vol. 58, pp. 925–929, July 1985.
[4] D. J. Seagle, S. H. Charap, and J. O. Artman, "Foldover in YIG," *J. Appl. Phys.*, vol. 57, pp. 3706–3708, Apr. 1985.
[5] Y. T. Zhang, C. E. Patton, and M. V. Kogekar, "Ferromagnetic resonance foldover in single crystal YIG films—Sample heating or Suhl instability," *IEEE Trans. Magn.*, vol. MAG-22, pp. 993–995, Sept. 1986.
[6] K. Gnatzig, H. Dötsch, and A. Brockmeyer, "Ferrimagnetic resonance in garnet films at large procession angles," *J. Appl. Phys.*, vol. 62, pp. 4839–4843, Dec. 1987.
[7] M. Chen, C. E. Patton, G. Shrinivasan, and Y. T. Yang, "Ferromagnetic resonance foldover and spin-wave instability in single-crystal YIG films," *IEEE Trans. Magn.*, vol. 25, pp. 3485–3487, Sept. 1989.
[8] Y. K. Fetisov, C. E. Patton, and V. T. Synogach, "Nonlinear ferromagnetic resonance and foldover in yttrium iron garnet thin films—Inadequacy of the classical model," *IEEE Trans. Magn.*, vol. 35, pp. 4511–4521, Nov. 1999.
[9] Y. K. Fetisov and C. E. Patton, "Microwave bistability in a nonlinear film ferromagnetic resonator," *J. Commun. Technol. Electron.*, pp. 664–669, June 2000. (Transl.: Radiotechnika i Electronika, vol. 45, pp. 735–741, June 2000).
[10] Y. K. Fetisov and A. V. Makovkin, "Nonlinear response of a bistable ferromagnetic resonator to a microwave pulse," *Tech. Phys.*, pp. 84–88, Jan. 2001. (Transl.: Zhurnal Technicheskoi Fiziki, vol. 71, pp. 86–91, Jan. 2001).
[11] H. M. Gibbs, *Optical Bistability. Controlling Light with Light*. New York: Academic, 1985.
[12] A. Prabhakar and D. D. Stancil, "Nonlinear microwave-magnetic resonator operated as a bistable device," *J. Appl. Phys.*, vol. 85, pp. 4859–4861, Apr. 1999.
[13] R. W. Damon and H. Van de Vaart, "Propagation of magnetostatic spin waves at microwave frequencies in a normally-magnetized disk," *J. Appl. Phys.*, vol. 36, pp. 3453–3459, 1965.
[14] R. J. Joseph and E. Schlömann, "Demagnetizing fields of nonellipsoidal bodies," *J. Appl. Phys.*, vol. 36, pp. 1579–1593, 1965.
[15] B. Lax and K. J. Button, *Microwave Ferrites and Ferrimagnetics*. New York, NY: McGraw-Hill, 1962.
[16] Y. K. Fetisov, I. V. Romanov, and V. B. Studenov, "Optical control of microwave signals in magnetostatic wave transmission line," *Electron. Lett.*, vol. 31, pp. 1168–1169, 1995.

Yuri K. Fetisov (SM'96) received the Ph.D. degree in solid state physics from the Moscow Engineering Physics Institute, Moscow, Russia, in 1981 and the Dr. Sci. degree in the physics of dielectrics and semiconductors from the Institute of Radioengineering and Electronics of Russian Academy of Sciences, Moscow, in 1993.

He joined the Moscow State Institute of Radioengineering, Electronics, and Automation (MIREA) as a Researcher in 1983. He was advanced to Professor in the Physics Department in 1994 and became Director of the Institute for Informatics in 1998. He has held visiting appointments in the Magnetics Laboratory of the Department of Physics at Colorado State University as a Visiting Professor in 1995, 1997, 1999, and 2001. His research group at MIREA is involved in magnetics research on ferromagnetic resonance, linear and nonlinear spin-wave processes in thin magnetic films, the magnetoelectric effect in multilayer composite structures, and design of solid state magnetic and microwave devices.

Prof. Fetisov is a Corresponding Member of the Russian Academy of Natural Sciences.

Carl E. Patton (SM'71–F'89) received the B.Sci. degree in physics from the Massachusetts Institute of Technology, Cambridge, and the M.Sci. and Ph.D. degrees in electrical engineering from the California Institute of Technology, Pasadena.

He was a Senior Research Scientist at Raytheon Research Division, Waltham, MA, from 1967 to 1971. He joined the Department of Physics at Colorado State University (CSU), Fort Collins, in 1971 as an Associate Professor and was advanced to Professor in 1976. His research group at CSU is involved in magnetics research on microwave and millimeter wave relaxation processes, Brillouin light scattering in magnetic films and superlattices, hexagonal ferrite materials, ferromagnetic resonance, nonlinear spin wave processes, and envelope solitons in thin films.

Prof. Patton is a Fellow of the American Physical Society. He was awarded an IEEE Third Millennium Medal in 2000 and received the IEEE Magnetics Society Lifetime Achievement Award in 2003. He has served as Editor of IEEE TRANSACTIONS ON MAGNETICS and as General or Publication Chair for several international magnetism conferences. He was Chair of the newly formed American Physical Society Topical Group on Magnetism and its Applications for 1998–1999. He is presently Secretary/Treasurer of the IEEE Magnetics Society. He is a member of the International Organizing Committee for the International Conference on Ferrites (ICF) and Program Chair for ICF9, August 2004, San Francisco, CA.